Zhang, B., *et al.*: Numerical Simulation of Droplet Impinging Icing Process ...
THERMAL SCIENCE: Year 2022, Vol. 26, No. 4B, pp. 3373-3385

3373

NUMERICAL SIMULATION OF DROPLET IMPINGING ICING PROCESS ON A LOW TEMPERATURE WALL WITH SMOOTHED PARTICLE HYDRODYNAMICS METHOD

by

Bowen ZHANG, Xiaojing MA*, Xinchao ZHOU, and Guangyuan LI

College of Electrical Engineering, Xinjiang University, Urumqi, China

Based on the basic principles and improved algorithms of the smoothed particle hydrodynamics method, a corresponding surface tension model and latent heat model are proposed for the heat exchange phase transition problem of droplets impinging on a low temperature wall surface. This research establishes a novel smoothed particle hydrodynamics model of the impinging wall of droplets accompanied by the phase transition process. This work also includes simulations covering the spreading flow and phase transition process of droplets under different impingement regimes. Moreover, the icing patterns of the droplet impingement spreading process are provided and a comparative analysis with related experimental results. The improved smoothed particle hydrodynamics model is verified by experiments and its ability to solve droplet impingement icing problems.

*Key words: smoothed particle hydrodynamics, droplet impingement,
phase transition, surface tension, numerical simulation*

Introduction

The icing process of droplets impinging on a low temperature wall is a common natural phenomenon that often occurs in various industrial productions. The phenomenon of water droplet icing often triggers accidents leading to major disaster when it appears in industries such as space and power networks. For example, ice accumulation can affect power transmission and the reliability of telecommunications networks [1]. Ice can seriously degrade aircraft performance and lead to plane crashes, yet, despite the advanced technology that assists in controlling ice accumulation on the outside of a plane, glaze icing is still a problem that is not fully understood [2]. Therefore, understanding water droplet icing is important to the success of abating or controlling ice accumulation in the future.

The icing process of droplet impinging on a low temperature wall is a complex process that is related to multidisciplinary knowledge. The process not only relates to the kinetic process of spreading against shrinking after a water droplet impinges on a wall but also relates to the thermodynamic process of heat transfer. At present, domestic and foreign scholars have made great progress in the study of the impingement of water droplets on solid walls at low temperatures. Smoothed particle hydrodynamic (SPH) methods, as a mesh-free Lagrange method, are often applied in the numerical simulation of free surface problems [3]. Zhang *et al.* [4] simulated the diffusion against the solidification process of droplets impinging on the wall surface in the molten state using the SPH method and analyzed the effect of different wall surface roughness levels on the droplet motion process. They further confirmed that the SPH method

---

3374

Zhang, B., *et al.*: Numerical Simulation of Droplet Impinging Icing Process ...
THERMAL SCIENCE: Year 2022, Vol. 26, No. 4B, pp. 3373-3385

is a powerful tool used to study droplet diffusion and solidification. Fang *et al.* [5] adopted a modified SPH model to numerically simulate the diffusion and solidification process of high Reynolds number droplet impingement wall surfaces and compared the motion morphology with the droplet impingement on wall surfaces as well as the solidification shape with a related experimental chart. Their results showed that the simulated chart was in approximate agreement with the experimental chart [5]. Chen *et al.* [6] carried out an experimental study on the solidification process of large droplets impinging on the wall surface and recorded the dynamic process of droplets impinging on the wall surface at different degrees of low temperatures using high speed imaging technology combined with infrared thermometry imaging. Hu *et al.* [7] used a high speed video camera to record the solidification process of water droplets impinging on the wall surface with different characteristics. Their analysis factored in the water droplet impingement velocity and wall temperature to compare material thermal conductivity with the freezing time of water droplets [7].

In this paper, based on the core idea of the SPH method and the principle of heat transformation, we propose a criterion for judging the phase transformation of droplets based on the latent thermal model. Both experimental and simulation results were used to develop a modified model of thermal conductivity considering ice shape when combined with a continuum surface force (CSF) model that reflects the hydrophobic characteristics of the wall. We also used modification techniques such as artificial viscosity, δ-SPH, and kernel gradient correction to construct an SPH model for the icing process of droplet impinging on a wall. Therefore, in this paper, the icing process of the droplet impinging on the low temperature wall surface is first simulated. The spreading process of the droplet, as well as the temperature change pattern of the icing on the bottom layer of the droplet, is analyzed, verified, and compared with experimental results. Next, the simulation study of the droplet phase transition process under different impingement working conditions was also conducted to analyze the influence of some factors, such as the impingement velocity, solid-liquid temperature differences, wall thermal conductivity, and the droplet surface tension coefficient on droplet spreading and icing processes.

Fundamental principle of smoothed particle hydrodynamics

The numerical simulation method is one of the most popular methods used to solve scientific and engineering problems. Usually, the simulation method is broadly divided into the grid method and grid-free method. Although the grid method is more widely used, it may encounter problems such as grid deformity when dealing with large and complex deformations, therefore, the grid-free method has been widely developed in recent years [3]. Unlike the grid method, the grid-free method employs a set of points to solve the region discretely, however, both methods can guarantee the precision of the calculation in simulation. The grid-free method also relies on calculations assisted by discrete points to construct approximate functions. This method can eliminate problems such as grid reconstruction when simulating large deformation problems, which helps when dealing with complex deformation problems such as hitting-wall splashes [8].

As a typical grid-free particle method, the SPH method proposed by Gingold and Monaghan is widely used among continuous solid mechanics and fluid mechanics. In the SPH method, the computational domain can be discretized into a group of particles with material properties that interact within the control range of a weight function or smooth function [9]. The integral expression of the field function is obtained by the approximation the kernel function, and the field function is further discretized as a summation of the particles within the support domain. The derivative form of the field function, as well as the field function, are expressed [9]:

$$\langle f(x) \rangle = \int_{\Omega} f(x')W(x-x',h)\mathrm{d}x' \tag{1}$$

$$\langle \nabla f(x) \rangle = \int_{\Omega} f(x')\nabla W(x-x',h)\mathrm{d}x' \tag{2}$$

where $\langle f(x) \rangle$ is the approximate number of $f(x)$, x – the position vector, Ω – the integrated volume containing x, h – the smoothing length, and W – the kernel function. The Gaussian kernel function is adopted:

$$W(R,h) = \alpha_d \mathrm{e}^{-R^2} \tag{3}$$

where $R = |x - x'|/h$, and the constant $\alpha_d = 1/\pi h^2$ for 2-D spaces.

The governing equations in the Lagrange form include the mass conservation equation, the momentum conservation equation, and the energy conservation equation which are represented in the SPH discrete form, which are expressed, respectively:

$$\frac{\mathrm{d}\rho_i}{\mathrm{d}t} = \rho_i \sum_{j=1}^{N} \frac{m_j}{\rho_j}(v_{ij}\nabla W_{ij}) \tag{4}$$

$$\frac{\mathrm{d}v_i}{\mathrm{d}t} = -\sum_{j=1}^{N} m_j \left(\frac{p_i}{\rho_i^2} + \frac{p_j}{\rho_j^2} \right) \nabla W_{ij} + \sum_{j=1}^{N} m_j \frac{(\mu_i + \mu_i)}{\rho_i \rho_j} \frac{x_{ij}\nabla W_{ij}}{|x_{ij}|^2} v_{ij} + f^{(s)} \tag{5}$$

$$m_i \frac{\mathrm{d}e_i}{\mathrm{d}t} = -\frac{1}{2}\sum_{j=1}^{N} m_i m_j (\frac{p_i}{\rho_i^2} + \frac{p_j}{\rho_j^2}):v_{ij}\nabla W_{ij} - \frac{1}{2}\sum_{j=1}^{N} \frac{m_i m_j(\mu_i + \mu_j)}{\rho_i \rho_j}\left(\frac{1}{x_{ij}}\nabla W_{ij} \right)v_{ij}^2 - \\ -\sum_{j=1}^{N} \frac{m_i m_j}{\rho_i \rho_j} \frac{(\lambda_i + \lambda_j)(T_i - T_j)}{x_{ij}^2}x_{ij}\nabla W_{ij} \tag{6}$$

where ρ, p, m, μ, λ, and T represent the density, pressure, mass, dynamic viscosity coefficient, thermal conductivity, and temperature, respectively. The $f(s)$ is the surface tension, i and j each represent different particles, and j particles are the neighboring particles within the i particle support domain. Therefore, v_{ij} and x_{ij} represent the velocity difference and distance between the i particles and j particles.

In our study, the fluid is viewed as a micro compressible fluid, with fluid pressure calculated using [10, 11]:

$$p_i = c^2(\rho_i - \rho_0) \tag{7}$$

where c is the velocity of sound. Notably, the value of the velocity of sound in this paper is 6-8 times the impingement velocity, whereas ρ_0 is the particle initial density.

A modified technique of the smoothed particle hydrodynamics method

Artificial viscosity model

To eliminate non-physical oscillations and particle penetration of the computational results within the impact domain, an artificial viscosity term, Π_{ij}, was added to the momentum equation. Thus, the momentum equation under the SPH form can be re-expressed:

$$\frac{\mathrm{d}v_i}{\mathrm{d}t} = \sum_{j=1}^{N} -m_j \left(\frac{p_i + p_j}{\rho_i \rho_j} + \Pi_{ij} \right) \nabla W_{ij} + \sum_{j=1}^{N} m_j \frac{(\mu_i + \mu_i)}{\rho_i \rho_j} \frac{x_{ij}\nabla W_{ij}}{|x_{ij}|^2}v_{ij} + f^{(s)} \tag{8}$$

3376

Zhang, B., *et al.*: Numerical Simulation of Droplet Impinging Icing Process ...
THERMAL SCIENCE: Year 2022, Vol. 26, No. 4B, pp. 3373-3385

$$\Pi_{ij} = \begin{cases} \dfrac{-\alpha_\Pi \overline{c_{ij}} \varphi_{ij} + \beta_\Pi \varphi_{ij}^2}{\overline{\rho_{ij}}} & v_{ij}x_{ij} < 0 \\[4pt] & v_{ij}x_{ij} \geq 0 \\[4pt] 0 \end{cases} \tag{9}$$

where $\varphi_{ij} = h_{ij}v_{ij}x_{ij}/(|x_{ij}|^2 + \phi^2)$, $\overline{c}_{ij} = (c_i + c_j/2,)$ $h_{ij} = (h_i + h_j)/2$, $\overline{\rho}_{ij} = \rho_i\rho_j/\rho_0$. To eliminate numerical divergence resulting from the proximity of particles to each other, ϕ is set to 0.1 h, and a_Π, and β_Π are the artificial viscosity coefficient. The low impingement velocity problem studied in this paper, a_Π, is set between 0 and 1, and β_Π is set to 0.

Kernel gradient correction

Conventional SPH methods suffer from insufficient precision in reproducing linear and quadratic functions. The issue of precision is closely related to the distribution and kernel function of particles. To improve the precision of the conventional SPH method, several approaches including reconstruction of the kernel function and construction of a Taylor expansion-based SPH approximation structure have been used successively in recent years. For the SPH approximation structure under Taylor's expanded form, the gradient of the smooth function affects the precision of the derivative approximation, and the use of the modified kernel gradient form can enhance the precision of the approximation [12]. Therefore, the modified kernel gradient formula should be written:

$$\nabla^C W_{ij} = L(r_i)\nabla W_{ij} \tag{10}$$

$$L(r_i) = \left(\sum_{j=1}^{N} \frac{m_j}{\rho_j} \nabla W_{ij} \otimes x_{ij} \right)^{-1} \tag{11}$$

Moreover, the governing equations can be re-written:

$$\frac{\mathrm{d}\rho_i}{\mathrm{d}t} = \rho_i \sum_{j=1}^{N} \frac{m_j}{\rho_j} v_{ij} \nabla^C W_{ij} \tag{12}$$

$$\frac{\mathrm{d}v_i}{\mathrm{d}t} = \sum_{j=1}^{N} -m_j \left(\frac{p_i + p_j}{\rho_i\rho_j} + \Pi \right)\nabla^C W_{ij} + \sum_{j=1}^{N} m_j \frac{(\mu_i + \mu_j)}{\rho_i\rho_j} \frac{x_{ij}\nabla^C W_{ij}}{|x_{ij}|^2} v_{ij} + f^{(s)} \tag{13}$$

$$m_i \frac{\mathrm{d}e_i}{\mathrm{d}t} = -\frac{1}{2} \sum_{j=1}^{N} m_i m_j \left(\frac{p_i}{\rho_i^2} + \frac{p_j}{\rho_j^2} \right) : v_{ij}\nabla^C W_{ij} - \frac{1}{2} \sum_{j=1}^{N} \frac{m_i m_j (\mu_i + \mu_j)}{\rho_i\rho_j} \left(\frac{1}{x_{ij}}\nabla^C W_{ij} \right) v_{ij}^2 -$$
$$-\sum_{j=1}^{N} \frac{m_i m_j}{\rho_i\rho_j} \frac{(\lambda_i + \lambda_j)(T_i - T_j)}{x_{ij}^2} x_{ij}\nabla^C W_{ij} \tag{14}$$

The δ-SPH

To overcome the false pressure fluctuation due to the speed reflection of sound, the δ-SPH model proposed by Colagrossi and Landrini was adopted in this study [13]. This model incorporates appropriate diffusion terms into the mass conservation equation eliminate high frequency oscillations that are prevalent in the pressure field. Upon addition of a density diffusion term, the mass conservation equation:

$$\frac{\mathrm{d}\rho}{\mathrm{d}t} = \rho_i \sum_{j}^{N} \frac{m_j}{\rho_j} v_{ij} \nabla^C_{\ i} W_{ij} + \rho_\delta \tag{15}$$

$$\rho_\delta = \delta h c \sum_j^N \frac{m_j}{\rho_j} \psi_{ij} \nabla^C_i W_{ij} \tag{16}$$

$$\psi_{ij} = 2(\rho_i - \rho_j)\frac{x_{ij}}{|x_{ij}|^2} \tag{17}$$

where the δ is usually set to 0.1.

Surface tension model

In the CSF model, the calculation of surface tension starts with defining a color function, proceeds through the value of the color function the surface normal vector and then to the surface curvature before the unit surface tension is finally derived.
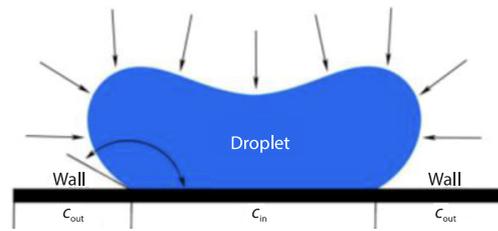

Figure 1. Schematic of surface tension

As shown in fig. 1, the color value of the droplet is defined as 1, the fraction of droplets in contact with the wall is c_{in}, and its value depends on the hydrophilicity and hydrophobicity of the wall surface. The wall part not in contact with the droplet is c_{out}, and its color value is 1 [14]:

$$c_{in} = 0, \quad c_{in} < M$$
$$c_{out} = 1, \quad c_{out} \geq M \tag{18}$$

The surface was located using a smooth color function:

$$\overline{c_{ij}} = \sum_{j=1}^N \frac{m_j}{\rho_j} c_j W_{ij} \tag{19}$$

The interfacial normal direction, as well as the curvature, was again calculated:

$$n_i = \sum_{j=1}^N \frac{m_j}{\rho_j}(\overline{c_j} - \overline{c_i})\nabla^C W_{ij} \tag{20}$$

$$\hat{n}_i = \begin{cases} \dfrac{n_i}{|n_i|} & ,|n_i| > \dfrac{0.01}{h} \\ 0 & ,\text{else} \end{cases} \tag{21}$$

$$k_i = -\sum_{j=1}^N \frac{m_j}{\rho_j}(\hat{n}_j - \hat{n}_i)\nabla^C W_{ij} \tag{22}$$

The final surface tension equation is presented:

$$F^{(s)} = -\frac{\sigma}{\rho_{ij}}(\nabla\hat{n})n_i \tag{23}$$

where σ is the surface tension coefficient.

For the problems studied in this paper, the value of M is related to the contact angle θ, and the value equation is shown [15]:

$$M = 0.0026\theta + 0.0461 \tag{24}$$

Treatment of solid wall boundary

In simulation studies, the material parameters of solid wall particles are consistent with droplet particles. In the computational domain, solid wall particles against droplet particles would participate in iterative calculations, but the location of the solid wall particles as well as some other material parameters would not change as the calculations progressed.

To prevent particle penetration from occurring when the droplet particles impinge on the wall-attached particles, an artificial repulsive force model proposed by Zhang and Liu [16] was adopted in the simulation study. The artificial repulsive force model is given:

$$f_{ij}^H = 0.01c^2 \chi f(n) \frac{x_{ij}}{\left|x_{ij}\right|^2}$$ (25)

$$\chi = 1 - \frac{\left|x_{ij}\right|}{\Delta d}, \quad 0 < \left|x_{ij}\right| < \Delta d$$ (26)

$$f(\eta) = \begin{cases} \dfrac{2}{3}, & 0 < \eta < \dfrac{2}{3} \\ (2\eta - 1.5\eta), & \dfrac{2}{3} < \eta \leq 1 \\ 0.5(2 - \eta), & 1 < \eta < 2 \\ 0, & \text{otherwise} \end{cases}$$ (27)

$$\eta = \frac{\left|x_{ij}\right|}{0.83h_{ij}}$$ (28)

where Δd is the initial interparticle spacing.

Phase transition model

We analyzed our phase transition model from an energy production point of view. The transformation of water from a liquid to a solid-state occurs roughly in three-stages. The first stage is the one that produces energy exchange due to the temperature differences, the second stage focuses on the latent heat required to overcome the phase transition, and the third phase represents the complete phase transition. Therefore, to realize the transition model process, a judgment criterion of the droplet phase transition based on the latent heat model was adopted in this study:

$$\begin{aligned} e > c_L T_m + L \quad &\text{liquid} \\ c_p T_m \leq e \leq c_p T_m + L \quad &\text{solidifying} \\ e < cp T_m \quad &\text{solid} \end{aligned}$$ (29)

where T_m is the melting temperature, L – the latent heat, and c_p – the specific heat capacity.

Because the specific heat capacities of the solid and liquid were quite different, the specific heat capacities in the phase transition process are solved and presented in fig. 2. As the water temperature gradually approached 0 °C, the icing of water began to occur, accompanied by a continuous decline in energy. However, due to the latent heat, the temperature of the water was maintained at 0 °C until complete solidification occurred. Therefore, c_p is viewed in this study as a linear change meant to achieve the aforementioned physical phenomena, as illustrated in fig. 2.

Figure 2. The c_p phase transition diagram
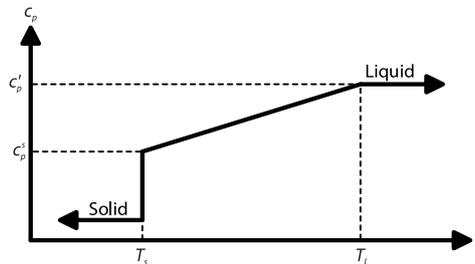
The previous description can be expressed:

$$c_p = \begin{cases} c_p^s & T < T_s \\ \dfrac{c_p^s + c_p^l}{2} + \dfrac{\Delta H}{T_i - T_s} & T_s \le T \le T_l \\ c_p^l & T > T_l \end{cases} \tag{30}$$

where ΔH is the latent heat.

Correction of heat transfer coefficient

Due to the different densities of water and ice, the shape and height of ice will change after the water drops completely change from the liquid phase to the solid phase. Therefore, according to the thermal conductivity of wall and ice and the influence factors of ice shape and ice height, the direct thermal resistance of wall and ice can be expressed [7]:

$$R = \frac{\alpha H}{2A}\left(\frac{1 - X_i}{\lambda_s} + \frac{X_i}{\lambda_i}\right) \tag{31}$$

where A is the solid-liquid contact area, H – the ice height, λ_s – the thermal conductivity of wall materials, and λ_i – the thermal conductivity of ice, X_i – the influence factor of the thermal conductivity of ice on the overall heat transfer efficiency, and a – the correction factor of the ice shape and ice height.

According to Fourier's law of heat conduction, thermal resistance can be expressed as the ratio of material length to the product of the thermal conductivity and the cross-sectional area of the heat flux direction. Then, the thermal conductivity of particles after the phase transition can be redefined:

$$\lambda = \frac{2}{\alpha\left(\dfrac{1 - X_i}{\lambda_s} + \dfrac{X_i}{\lambda_i}\right)} \tag{32}$$

where the value of the ice shape and ice height correction coefficient α an empirical value obtained from repeated experiments. For example, the values obtained by Hu *et al.* [7] is 1.05-1.25. Based on the analysis of repeated simulation results, we found that the value α has a certain relationship with the velocity of the droplet impacting the wall. Thus, the value of α can be expressed:

$$\alpha = \alpha_0\left(\frac{v_0}{2}\right)^{-0.99} \tag{33}$$

where the value of α_0 is between 1.05 and 1.25.

3380

Zhang, B., *et al.*: Numerical Simulation of Droplet Impinging Icing Process ...
THERMAL SCIENCE: Year 2022, Vol. 26, No. 4B, pp. 3373-3385

Velocity correction

In general, the velocity of a single particle is not significantly different from that of the surrounding particle. Therefore, the velocity correction technology was used in the research to avoid the obvious difference between the velocity of a single particle and the velocity of surrounding particles in the simulation process, which makes the simulation results more precise. The velocity correction formula [17]:

$$v_i = v_i - \overline{\beta} \sum_{j=1}^{N} \frac{m_j v_{ij} W_{ij}}{\dfrac{\rho_i + \rho_j}{2}} \tag{34}$$

where $\overline{\beta}$ is the correction coefficient and we set the value of $\overline{\beta}$ to 0.05 in this study.

Time integral scheme

To get the physical change of each particle, the predictive correction integral algorithm is used to integrate the differential equation. The first-half change of particles is predicted [18]:

$$\rho_i^{n+1/2} = \rho_i^n + \frac{\Delta t}{2} \frac{d\rho_i^n}{dt}, \; v_i^{n+1/2} = v_i^n + \frac{\Delta t}{2} \frac{dv_i^n}{dt}, \; x_i^{n+1/2} = x_i^n + \frac{\Delta t}{2} v_i^n \tag{35}$$

Then, the second half change of the particle is predicted:

$$\overline{\rho}_i^{n+1/2} = \rho_i^n + \frac{\Delta t}{2} \frac{d\rho_i^{n+1/2}}{dt}, \; \overline{v}_i^{n+1/2} = v_i^n + \frac{\Delta t}{2} \frac{dv_i^{n+1/2}}{dt}, \; \overline{x}_i^{n+1/2} = x_i^n + \frac{\Delta t}{2} v_i^{n+1/2} \tag{36}$$

To ensure the stability of numerical simulation, the time step should meet the Courant-Friedrichs-Lewy condition, the viscous condition, and the mass force condition [19]:

$$\Delta t \le \min\left[\frac{h}{c}, \left(\frac{h}{f} \right), \frac{0.5h\,\rho}{\mu} \right] \tag{37}$$

where f is the force per unit mass.

Numerical example verification

In order to verify the validity and precision of the model based on the improved SPH method, we analyzed the movement state, temperature change, and icing time of droplets in the early stage of droplet impact phase transition. As a result, we obtained the corresponding pattern and finally compared that data with the experimental results.

Model validation of phase transition process
of droplet impinging on wall

For comparison and analysis, the parameters of droplet size and wall material are identical with the experimental data of Hu *et al*. [7]. The droplet radius is $1.3 \cdot 10^{-3}$ m. The impingement velocity of the water droplets is 1 m/s, 1.4 m/s, 1.7 m/s, and 2 m/s, in that order. The wall material is still aluminum, and the wall temperature is –25 °C. Figure 3 shows the cloud chart of the droplet icing at different impingement velocities. We can observe from fig. 3 that the solidification process of the droplet starts from the bottom and gradually solidifies upward with the passage of time until the whole droplet is completely frozen. The higher the impingement velocity of the droplets, the more obvious the tendency is for the droplets to extend to both sides, and the faster the icing speed of the droplets.
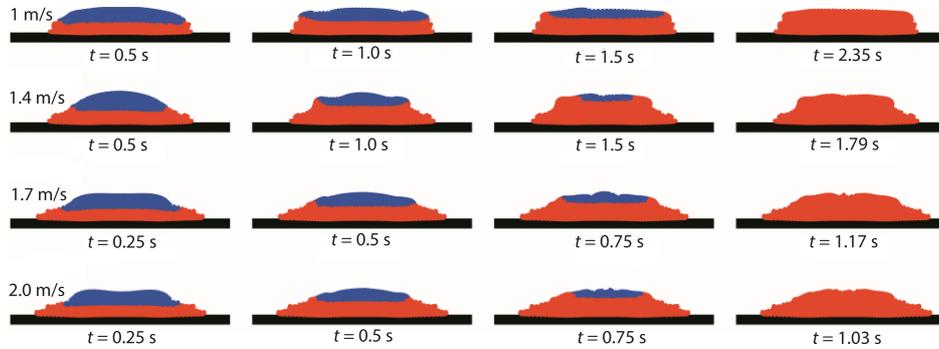
Zhang, B., *et al.*: Numerical Simulation of Droplet Impinging Icing Process ...
THERMAL SCIENCE: Year 2022, Vol. 26, No. 4B, pp. 3373-3385

3381

Figure 3. Cloud chart of droplet icing (the red part is frozen, the blue part is not frozen)

– Icing time of droplet

In the study of the water droplet phase transition, the icing time is an extremely important index. Icing times are compared in fig. 4. With the increase of droplet impingement velocity, the icing time of the droplet decreased correspondingly. Figure 4 shows that the icing time of the water droplet with an impingement velocity of 1 m/s is different from the experimental results. In addition this velocity, the other icing times of different droplet impingement velocities were in good agreement with the experimental results.

– Spreading pattern of droplets

In order to understand the movement process of a water droplet hitting the wall surface directly, the maximum spreading coefficient of the water droplet is taken as the characteristic parameter in this paper. When the radius of the droplet and the wall parameters remain unchanged, we recorded the maximum spreading coefficient at different impingement velocities. The maximum spreading coefficient can be defined as the ratio of the maximum spreading radius $R(t)$ to the initial radius Rd, and the results are shown in fig. 5.
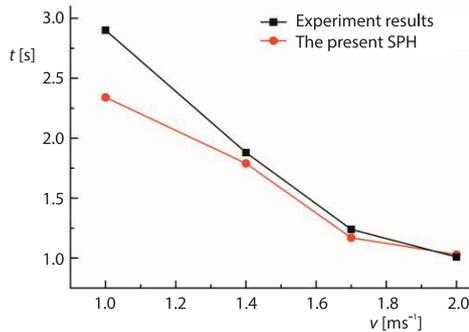

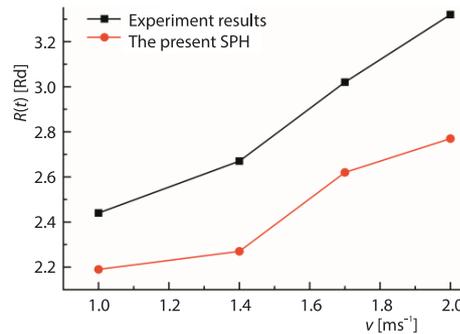**Figure 4. Droplet icing time curve (aluminium)**

Figure 5. Comparison curve of spreading coefficients

In order to maintain the stability of the simulation results, after the water particles are completely transformed into ice particles, a method similar to solid wall boundary treatment was adopted for ice particles. Ice particles are involved in the calculation, but the position of ice particles did not change, which results in the phase transformation process of the bottom water particles before the spreading is completed, which prevents the further spreading of the particles. Therefore, as shown in fig. 5, the maximum spreading coefficient obtained by simulation is similar to that obtained by experiment.

– Temperature distribution of droplets

In order to further verify the validity of the model and to study the initial icing stage of the droplets, the temperature distribution of droplets is also studied in this paper. To compare with the experiment, the experimental data of Chen *et al.* [6] were used for numerical simulation. In this experiment, the size of the wall is $2 \cdot 10^{-2}$ m $\times$ $3.125 \cdot 10^{-4}$ m, the radius of the water droplet is $1 \cdot 10^{-3}$ m, the initial particle radius is $6.25 \cdot 10^{-5}$ m. The initial velocity of the droplet is 2.1 m/s and the contact angle is 60 °. The wall material is aluminum; the thermal conductivity is 237 W/mK; the wall temperature is − 20 °C, and the initial droplet temperature is 20 °C. The temperature change of the droplet's lowest layer particles is shown in fig. 6(a).
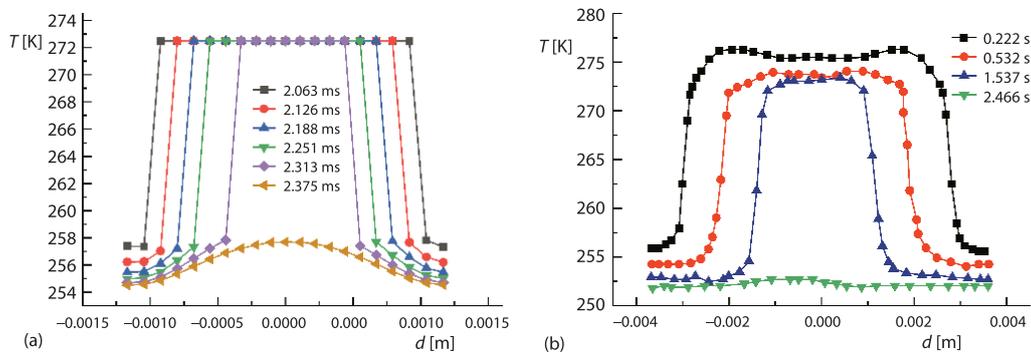

Figure 6. Simulation results of (a) lower layer temperature and (b) experimental results

Figure 7. Cloud charts of droplet freezing under different temperatures; (a) 1.0 m/s cloud chart of frozen droplets, (b) 1.7 m/s cloud chart of frozen droplets, and (c) 2.0 m/s cloud chart of frozen droplets

Figure 6 shows that after the spreading and shrinking of water droplets, the bottom layer temperature of water droplets decreases continuously, and the phase transformation process expands from the edge to the middle. After the phase transformation of water is completed, the ice temperature continues to decrease until it is close to the wall temperature. The experimental results obtained by Chen *et al.* [6] are shown in fig. 6(b). Clearly, the temperature distribution of the experimental results is similar to that of the simulation results.

Influence of wall temperature on
the phase transformation of droplet

The experimental results show that the temperature differences between the solid and liquid is the main factor affecting the phase transition of the droplet impact. Therefore, we studied the phase transition process of droplets by changing their wall temperatures in this paper. In order to compare with the experimental results, the simulation example is consistent with the experimental data of Hu *et al.* [7]. In this example, the experimental data of [7] were still used to build the simulation model. The wall material is copper, the thermal conductivity is 401 W/mK, and the wall temperature is −15 °C, −25 °C, and –35 °C in that order. Figure 7 shows the spreading and icing process of droplets at different temperatures, and fig. 8 shows the curve of the icing time.
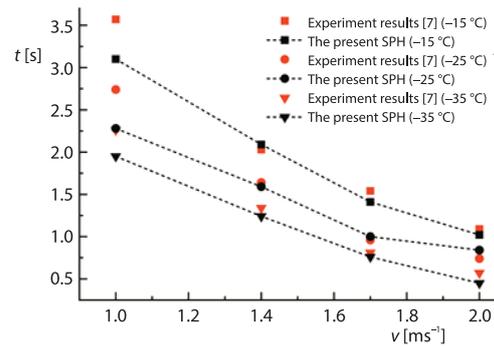

Figure 8. Icing time curve (Cu)

Figure 7 shows that the lower the wall temperature is, the shorter the icing time of the droplet is when the droplet impingement velocity remains the same. The same phenomenon can be seen in fig. 8. In this case, no matter what the simulation results or the experimental results, the increase of the solid-liquid temperature difference will greatly affect the icing process of the droplets.

Influence of droplet surface tension coefficient
on the phase transformation of droplet

In order to further study the influence of the physical parameters of droplets in the icing process, the same model and data are used in this example, and the temperature differences between the solid and liquid is controlled up to 100 °C. By changing the surface tension coefficient of the droplets, the law of surface tension coefficient and icing time is obtained, as shown in fig. 10, where the surface tension coefficient is expressed by the Weber number. The $We = \rho v^2 l/\sigma$, where l is the characteristic length, and the value is the diameter of the droplet. Figure 9 shows the freezing of droplets with different Weber numbers.
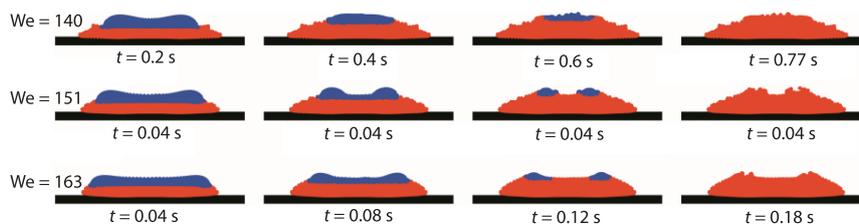

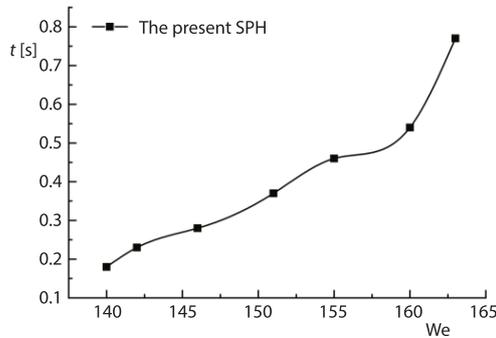**Figure 9. Cloud charts of droplet freezing under different Weber numbers**

3384

Zhang, B., *et al.*: Numerical Simulation of Droplet Impinging Icing Process ...
THERMAL SCIENCE: Year 2022, Vol. 26, No. 4B, pp. 3373-3385

Figure 10. Icing time curve (Weber number)

Figure 9 shows that the freezing speed of high Weber number droplet is obviously faster than that of low Weber number droplet under the same range of temperature. As shown in fig. 10, with the increase of the Weber number, the icing time obviously increases, which also shows that the surface tension coefficient as one of the factors that affects the solidification of droplets.

Conclusions

In this paper, the improved SPH method was used to simulate the dynamic process of the phase transition of droplet impinging on the wall. After analyzing the results, we came to the following conclusions.

- According to the basic principles of SPH and heat transfer, a criterion of phase transition is proposed in this paper. The specific heat capacity and thermal conductivity of the droplet are modified. Based on this, a numerical model of SPH considering the phase transition process is established by combining the CSF model and δ-SPH correction techniques.
- To verify the validity of the SPH numerical model, the droplet impact phase transition process was simulated. The temperature distribution of the bottom layer at the initial icing stage of the droplet, the icing time of the droplet under different impingement velocities, and the shape change of the droplet were analyzed. The simulation results are in good agreement with the experimental results.
- On the basis of the experiments and the simulated SPH model, the authors also simulated droplet spreading and icing patterns under different solid-liquid temperature differences, and compared with the experimental results. The results show that the temperature difference between a solid and liquid is an important factor affecting the freezing of droplets. In order to further explore the influencing factors of droplet icing, this paper also simulated the influence of different surface tension coefficients on droplet icing. The simulation results show that the surface tension coefficient has an impact on the icing time of droplets to a certain extent.

Nomenclature

A – solid-liquid contact area, [m^2]
c_p – specific heat capacity, [Jkg^{-1}K^{-1}]
H – ice height, [m]
h – smoothing length, [m]
L – latent heat, [J]
m – mass, [kg]
p – pressure, [Pa]
T – temperature, [K]
t – time, [s]
v – velocity, [ms^{-1}]
W – kernel function, [–]

We – weber number, [–]
X_i – influence factor of thermal conductivity, [–]
x – distance between particles, [m]

Greek symbols

α – correction factor of the ice shape
         and ice height, [–]
α_Π, β_Π – artificial viscosity coefficient, [–]
λ – thermal conductivity, [Wm^{-1}K^{-1}]
ρ – density, [kgm^{-3}]
σ – surface tension coefficient, [Nm^{-1}]

References

[1] Laforte, J. L., *et al.*, State-of-the-Art on Power Line de-Icing, *Atmospheric Research*, *46* (1998), 1, pp. 143-158

[2] Kind, R. J., *et al.*, Experimental and Computational Simulation of in-Flight Icing Phenomena, Progress in Aerospace Sciences, *34* (1998), 5, pp. 257-345

[3] Monaghan, J. J., *et al.*, Solidification Using Smoothed Particle Hydrodynamics, *Journal of Computational Physics*, *206* (2004), 2, pp. 684-705

[4] Zhang, M. Y., *et al.*, Application of Smoothed Particle Hydrodynamics Method to Free Surface and Solidification Problems, *Numerical Heat Transfer, Part A: Applications*, *52* (2007), 4, pp. 299-314

[5] Fang, H. S., *et al.*, Simulations of Droplet Spreading and Solidification Using an Improved SPH Model, *Numerical Heat Transfer, Part A: Applications*, *55* (2009), 2, pp. 124-143

[6] Chen, J., *et al.*, Unsteady Heat Transfer of Large Droplet Icing and Deicing Process Using Dielectric Barrier Discharge (in Chinese), *CIESC Journal*, *69* (2018), 9, pp. 3825-3834

[7] Hu, H. B., *et al.*, Freezing Behavior of Droplet Impacting on Cold Surfaces (in Chinese), *Acta Physica Sinica*, *65* (2016), 10, pp. 196-201

[8] Ma, X. J., *et al.*, Investigations of the Hydraulic Characteristics of Stilling Basin with Baffle-Blocks Using an Integrated SPH Method, *International Journal of Computational Methods*, *17* (2020), 08, pp. 109-117

[9] Liu, M. B., Liu, G. R. Smoothed Particle Hydrodynamics (SPH): an Overview and Recent Developments, *Archives of Computational Methods in Engineering*, *17* (2010), 1, pp. 25-76

[10] Morris, J. P., *et al.*, Modelling Low Reynolds Number Incompressible Flows Using SPH, *Journal of Computational Physics*, *136* (1997), 1, pp. 214-226

[11] Liu M. B., Li, S. H., On the Modelling of Viscous Incompressible Flows with Smoothed Particle Hydro-Dynamics, *Journal of Hydrodynamics*, Ser. B, *28* (2016), 5. pp. 731-745

[12] Shao, J. R., et al., An Improved SPH Method for Modelling Liquid Sloshing Dynamics, *Computers & Structures*, *100-101* (2012), June, pp. 18-26

[13] Colagrossi, A., Landrini, M., Numerical Simulation of Interfacial Flows by Smoothed Particle Hydrodynamics, *Journal of Computational Physics*, *191* (2003), 2, pp. 448-475

[14] Qiang, H. F., *et al.*, Smoothed Particle Hydrodynamics Method with Modified Surface Tension and Its Implementation, *Chinese Journal of Computational Physics*, *28* (2011), 3, pp. 375-384

[15] Li, G. Y., *et al.*, An Integrated Smoothed Particle Hydrodynamics Method for Numerical Simulation of the Droplet Impacting with Heat Transfer, *Engineering Analysis with Boundary Elements*, *124* (2021), Mar., pp. 1-13

[16] Zhang, Z. L., Liu, M. B., A Decoupled Finite Particle Method for Modelling Incompressible Flows with Free Surfaces, *Applied Mathematical Modelling*, *60* (2018), Apr., pp. 606-633

[17] Monaghan, J. J., On the Problem of Penetration in Particle Methods, *Journal of Computational Physics 82* (1989), 1, pp. 1-15

[18] Huang, C., *et al.*, Coupled Finite Particle Method with a Modified Particle Shifting Technology, *International Journal for Numerical Methods in Engineering*, *113* (2018), 2, pp 179-207

[19] Liu, M. B., Zhang, Z. L., Smoothed Particle Hydrodynamics (SPH) for Modelling Fluid-Structure Interactions, *Mechanics and Astronomy*, *60* (2019), 8, pp. 5-42